ingegneria sismica
International Journal of Earthquake Engineering
Anno XLIII - Num. 3 - 2026

Study on cooperative optimization calculation method of multiple grid-connected control parameters of photovoltaic power plant considering coordination of inertia and damping response characteristics

Lihui Tian[1,*]

[1] College of Electrical Engineering, Shanghai University of Electric Power, Shanghai 200090, Shanghai, China.

SUMMARY: *With the rapid development of renewable energy power generation, the penetration of distributed power sources in the power grid is rapidly increasing, and the microgrid with power electronic inverter as the interface leads to reduced system stability due to the lack of inertia and damping. In this paper, in order to make the photovoltaic power plant effectively support the grid operation, the virtual synchronous motor algorithm VSG is introduced into the control of the inverter, and in order to improve the dynamic characteristics of the system, the virtual impedance is added into the control of the virtual synchronous machine, and then the cooperative adaptive control strategy of inertia and damping is obtained by improving the traditional VSG control strategy, and the parameters of the adaptive control system are determined, so that the VSG has good and consistent stability in the power grid before and after the grid strength change before and after has a better and consistent response characteristics. Through MATLAB/Simulink simulation and comparison experiments, the results show that the adaptive control strategy proposed in this paper can not only inhibit the speed of frequency change, but also reduce the amount of frequency deviation, and the designed control strategy can effectively improve the transient response time of the system, which verifies the reasonableness and validity of the designed model and control strategy.*

KEYWORDS: *virtual synchronous generator; virtual inertia; damping coefficient; photovoltaic grid; adaptive control*

1 Introduction

In the 21st century, the structure of the world's energy resources has undergone a great change. With the severe shortage of traditional energy sources such as coal, oil and natural gas, mankind has shifted the direction of energy development to renewable energy. The large-scale development and utilization of renewable energy sources, and the diversified energy structure dominated by clean and clean renewable energy sources with unlimited resources instead of the energy structure dominated by traditional fossil energy sources with serious pollution and limited resources have turned into the focus of people's attention [1-3]. As a new type of green renewable energy, solar energy is the most ideal renewable energy source with the greatest utilization compared with other new energy sources. Especially in recent decades, with the continuous progress of science and technology, solar energy and its related industries have become one of the fastest growing industries in the world, and photovoltaic (PV) power

*tlhsheep123@163.com
https://doi.org/10.65102/is20261239
Published: 10 June, 2026

generation, as a kind of clean, safe, and reliable distributed energy source, has been receiving more and more attention and emphasis [4, 5].

There exist two working modes of PV power plants, off-grid and grid-connected. Previously, because of the high cost of producing solar cells, the application of PV power generation is often limited to remote areas without electricity, and most of them are small and medium-sized systems for households and villages, who are off-grid users [6]. However, in recent years, the photovoltaic industry and its market has changed a lot, the photovoltaic industry from remote rural areas gradually to the direction of photovoltaic building integration and urban grid-connected power generation rapid development, solar energy has been globally by the "complementary energy" role is recognized to be the next generation of "alternative energy" [7-9]. Grid-connected photovoltaic power plant, on the one hand, can be reasonable deployment and storage of electric energy, so that energy is maximized. On the other hand, the introduction of PV power generation into households and enterprises through grid-connection can reduce the dependence on traditional energy sources, thus reducing the expenditure on electricity [10, 11].

However, the low inertia problem brought about by large-scale grid-connected PV power plants has become a key hidden problem affecting the stability of power systems [12]. Traditional thermal generating units store kinetic energy through synchronous generator rotor rotation, and when the grid frequency fluctuations, these rotating bodies release or absorb energy to maintain system stability, like an invisible stabilizer for the grid, but PV power generation is connected to the grid through inverters, and this power electronic equipment does not have physical rotating parts to provide mechanical inertia support in the traditional sense [13-15]. When the PV penetration rate exceeds 30%, the system equivalent inertia may plummet by more than 60% [16]. In addition, in practice, an important problem facing grid-connected PV power plants is low damping [17]. Damping refers to the damping characteristics of various damping elements, sensors, controllers, etc., in PV grid-connected power generation. Under multiple grid-connected PV power plants, it is difficult to balance inertia support and damping enhancement [18, 19]. The actual operation data of some power grids show that the frequency regulation pressure increases by 2.3 times and the frequency fluctuation amplitude enlarges by 47% compared with the traditional operation mode during the midday PV power hour. In a regional grid fault in summer, the frequency collapse accident caused by inertia and damping insufficiency resulted in a direct economic loss of more than 80 million yuan. Therefore, how to coordinate the inertia and damping parameters to optimize the grid-connected control of photovoltaic power plants is an issue of concern.

This paper proposes an adaptive virtual inertia and damping cooperative control strategy based on VSG, and establishes the relationship between the virtual rotational inertia, damping coefficient and the system frequency deviation and frequency change rate. The inverter controlled by VSG can be equivalent to a synchronous generator, while the PV power supply is equivalent to a prime mover, and then simulate the characteristics of the synchronous generator power generation system, analyze the feasibility of the control strategy proposed in this paper then and determine the parameters of the adaptive control system. Finally, the influence of the regulation coefficients on the system performance is analyzed through MATLAB/Simulink simulation to verify the feasibility of the synergistic adaptive control strategy of rotational inertia and damping coefficients.

2 Co-optimization model for multiple grid-connected control parameters of PV power plants

2.1 Modeling of PV power plant system

2.1.1 Grid-connected photovoltaic systems

Grid-connected photovoltaic power generation system does not go through battery storage and directly inputs power into the large power grid through grid-connected inverter, its design structure mainly consists of devices such as photovoltaic arrays, grid-connected inverters and controllers [20]. The DC-DC converter and DC-AC inverter are utilized to invert the DC power into AC power, which is finally fed into the power grid. Grid-connected photovoltaic power generation system, compared with off-grid type, saves the battery pack charging and discharging links, not only reduces the loss caused by energy exchange, but also reduces the equipment land area, and more importantly, saves the construction cost. It can also be divided into decentralized grid-connected and centralized grid-connected.

Decentralized grid-connection: Also known as distributed grid-connection, the power generated is supplied directly to the load. If there is a surplus of power generated, the excess power is fed into the grid; if there is a shortage of power generated, the grid makes up for the surplus. It can be seen that two-way conduction can be realized between the power grid and the power generation system. This system is suitable for urban buildings and self-sufficient small-scale PV power generation systems.

Centralized grid-connected: It is to input the power output from the inverter directly into the public grid, and then uniformly transmitted and deployed by the grid. It can be seen that the system and the public grid can not realize the two-way conduction, only one-way transmission, so in the desert area of the large-scale PV power plant is usually used in this way for grid connection.

2.1.2 Mathematical modeling of PV cells and PV arrays

In this paper, a centralized grid-connected PV power system structure is used. The equivalent circuit diagram of the photovoltaic cell is shown in Fig. 1.

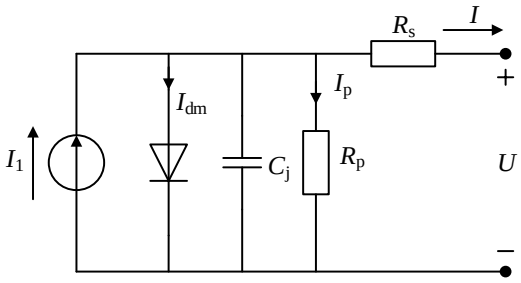

Figure 1: Equivalent circuit of photovoltaic cell

where I_1 is the photogenerated current; R_s and R_p are the series-parallel equivalent resistances in the cell, respectively; I and U are the output current and output voltage, respectively; C_j is the junction capacitance of the photovoltaic cell, and this branch current is negligible. I_{dm} is the forward current of the equivalent diode P-N junction under the external voltage when there is no light irradiation; I_p is the parallel branch current. From this, the output characteristic equation of the PV cell can be obtained:

$$\begin{aligned} I &= I_1 - I_{dm} - I_p \\ &= I_1 - I_0\left[\exp\left(\frac{(U+IR_s)q}{nkT}\right)-1\right] - \frac{U+IR_s}{R_p} \end{aligned} \tag{1}$$

where I_0 is the diode reverse saturation current; T is the current temperature; q has a value of 1.602×10^{-19}, and k has a value of 1.38×10^{-23}, both of which are constants; n is the diode factor, and ideally, n is 1. Eq. (1) requires further simplification:

Typically, the value of R_p is so large that the I_p term can be ignored; since the value of R_s is much less than the value of the diode's forward conduction resistance, it is possible to make $I_1 \approx I_{sc}$. The simplified mathematical model of the PV cell is as follows:

$$I = I_{sc}\left\{1 - C_1\left[\exp\left(\frac{U}{C_2U_{oc}}-1\right)\right]\right\} \tag{2}$$

where $C_1 = \left(1-\frac{I_m}{I_{sc}}\right)\exp\left(-\frac{U_m}{C_2U_{oc}}\right)$, $C_2 = \frac{\left(\frac{U_m}{U_{oc}}-1\right)}{\ln\left(1-\frac{I_m}{I_{sc}}\right)}$.

However, the above model presupposes that the temperature and light intensity are kept constant and does not take into account the output characteristics in case of changes in environmental factors. Therefore Eq. (2) is further modified:

$$\begin{cases} \Delta T = T - T_0 \\ \Delta S = \dfrac{S}{S_0} - 1 \\ I'_{sc} = \dfrac{I_{sc}\times S}{S_0}\left(1+a\Delta T\right) \\ U'_{oc} = U_{oc}\left(1+b\Delta S\right)\left(1-c\Delta T\right) \\ I'_m = \dfrac{I_m\times S}{S_0}\left(1+a\Delta T\right) \\ U'_m = U_m\left(1+b\Delta S\right)\left(1-c\Delta T\right) \end{cases} \tag{3}$$

where T_0 and S_0 are $25^\circ C$ and $1000W/m^2$; T and S denote the temperature and light intensity of the current environment, respectively; and a, b and c are the compensation coefficients. Then the modified PV cell output characteristic equation is:

$$I = I'_{sc}\left\{1 - C_1\left[\exp\left(\frac{U}{C_2U'_{oc}}-1\right)\right]\right\} \tag{4}$$

The corrected model obtained for engineering purposes does not require intricate parameters, and only four basic parameters provided by the PV cell manufacturer are needed to

build a mathematical model of the PV cell.

2.1.3 PV Grid-tied Inverter Control Structure and Modulation Methods

In power systems, inverters are key devices that connect distributed power sources to the larger grid. In the research and analysis of power systems, grid-connected inverters are usually three-phase voltage source PWM inverters. In this section, we will start from the elaboration of several classical outer-loop and voltage-current control strategies to select the inverter outer-loop and inner-loop control strategies suitable for the characteristics of large-scale PV power plants.

(1) Inverter outer-loop control strategy

The outer-loop control strategy determines the role of the inverter in the microgrid, and then the classical outer-loop control strategy of the inverter is analyzed with the line transmission characteristics. In order to analyze the grid-connection process of the inverter in depth, the inverter is equivalent to a controlled voltage source, and the grid-connection schematic diagram of the inverter after the equivalence is shown in Fig. 2.

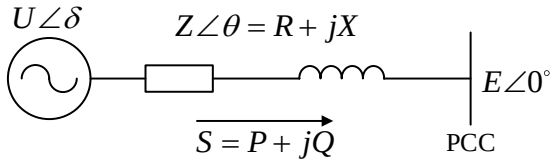

Figure 2: Grid-connected equivalent schematic diagram of inverter

where U and δ denote the output voltage of the inverter and its phase angle, respectively; E is the AC bus voltage; Z and θ denote the line impedance and its phase angle. According to Fig. 2, the inverter output power equation and line impedance relationship can be derived:

$$\begin{cases} P = \dfrac{EU\cos\delta\cos\theta - E^2\cos\theta + EU\sin\delta\sin\theta}{Z} \\ Q = \dfrac{EU\cos\delta\sin\theta - E^2\sin\theta - EU\sin\delta\cos\theta}{Z} \\ \sin\theta = \dfrac{X}{Z} = \dfrac{X}{\sqrt{R^2 + X^2}} \\ \cos\theta = \dfrac{R}{Z} = \dfrac{R}{\sqrt{R^2 + X^2}} \end{cases} \tag{5}$$

Organizing equation (5), the formula for the inverter output power becomes:

$$\begin{cases} P = \dfrac{E}{R^2 + X^2}\left[R(U\cos\delta - E) + XU\sin\delta\right] \\ Q = \dfrac{E}{R^2 + X^2}\left[X(U\cos\delta - E) - RU\sin\delta\right] \end{cases} \tag{6}$$

It can be seen that there is a relationship between the voltage magnitude and phase angle of the inverter and AC bus and the output power of the inverter.

(2) Inverter voltage-current inner loop control method

The purpose of voltage-current inner-loop control is mainly to accurately regulate the current and improve the power quality. The inner-loop control is usually divided into $dq0$ rotating coordinate system, $\alpha\beta 0$ stationary coordinate system and abc natural coordinate system, this paper completes the voltage and current inner-loop control through the mutual transformation of abc natural coordinate system and $dq0$ rotating coordinate system.

The control process of voltage-current inner loop is as follows: three-phase reference voltages u_{aref}, u_{bref} and u_{cref} are transformed by dq to generate two-phase reference voltages u_{dref} and u_{qref}, and u_d and u_q, which are introduced as the feedbacks to the voltage loop, and the difference of the two values is transformed by a proportional-integral (PI) controller. The proportional-integral (PI) controller introduces a cross-compensation link to decouple the dq components of the voltage and generate the current loop reference signals i_{dref} and i_{qref}. The PI controller is used to improve the dynamic response of the system.

2.2 Mathematical model of synchronous virtual generator

2.2.1 Electrical mathematical modeling of synchronous generators

$i_a i_b i_c$ and $\Psi_a \Psi_b \Psi_c$ are the currents and magnetic chains of the three-phase stator, respectively; i_f and Ψ_f are the currents and chains of the excitation winding, respectively, and the equations of the magnetic chains of stator winding and excitation winding are:

$$\Psi = \begin{bmatrix} \Psi_s \\ \Psi_f \end{bmatrix} = \begin{bmatrix} L_{aa} & M_{ab} & M_{ac} & L_{af} \\ M_{ba} & L_{bb} & M_{bc} & L_{bf} \\ M_{ca} & M_{cb} & L_{cc} & L_{cf} \\ L_{af} & L_{bf} & L_{cf} & L_{ff} \end{bmatrix} \begin{bmatrix} i_a \\ i_b \\ i_c \\ i_d \end{bmatrix} \tag{7}$$

where $\Psi_s = \left[\Psi_a \Psi_b \Psi_c\right]^T$, and L_{aa}, L_{bb}, and L_{cc} are the self-inductance of each phase of the stator, respectively, which are set to be of the same size L; M_{ab}, M_{bc}, and M_{ac} are the mutual inductances between the phases of the stator, which are set to be of the same magnitude $-M\left(M>0, M=0.5L\right)$ due to the difference in phase angles 120°; L_{ff} is the rotor self-inductance, set to L_f; the mutual inductance M_{af}, M_{bf}, and M_{cf} between the excitation and stator windings fluctuates according to a sinusoidal law as the rotor deviates from the a-phase by an electrical angle θ:

$$\begin{cases} M_{af} = M_f \cos\theta_a = M_f \cos\theta_a \\ M_{bf} = M_f \cos\theta_b = M_f \cos\left(\theta_a - \dfrac{2}{3}\pi\right) \\ M_{cf} = M_f \cos\theta_c = M_f \cos\left(\theta_a - \dfrac{4}{3}\pi\right) \end{cases} \tag{8}$$

Let $\cos\theta = \begin{bmatrix} \cos\theta_a \\ \cos\theta_b \\ \cos\theta_c \end{bmatrix}$, $\sin\theta = \begin{bmatrix} \sin\theta_a \\ \sin\theta_b \\ \sin\theta_c \end{bmatrix}$, $L = L_s + M$, the magnetic chain equation can be rewritten as:

$$\Psi = \begin{cases} \Psi_s = M_f i_f \cos\theta + L_s i_{abc} \\ \Psi_f = M_f i_{abc} \cdot \cos\theta + L_f i_f \end{cases} \tag{9}$$

Rotor excitation voltage:

$$\begin{bmatrix} u_{abc} \\ u_f \end{bmatrix} = \begin{bmatrix} R_s & 0 \\ 0 & u_f \end{bmatrix} \begin{bmatrix} i_{abc} \\ i_f \end{bmatrix} - \frac{d}{dt} \begin{bmatrix} \Psi_s \\ -\Psi_f \end{bmatrix} \tag{10}$$

where u_{abc} and i_{abc} are the terminal voltage $[u_a u_b u_c]^T$ and terminal current $[i_a i_b i_c]^T$ of each phase of the stator winding, respectively, and R_s is the stator winding resistance, so there is:

$$u_{abc} = -R_s i_{abc} - L_s \frac{di_{abc}}{dt} + e_{abc} \tag{11}$$

The reaction electromotive force e_{abc} generated by a synchronous generator in the stator winding can be viewed as a two-part system consisting of the line impedance voltage drop and the terminal voltage as:

$$e_{abc} = M_f i_f \dot{\theta} \sin\theta - M_f \frac{di_f}{dt} \cos\theta \tag{12}$$

where $\dot{\theta}$ is the rotor angular frequency, when the synchronous generator operation into the steady state after the excitation current i_f remains unchanged, that is, $di_f / dt = 0$, then (12) can be simplified as:

$$e_{abc} = \omega M_f i_f \sin\theta = \sqrt{2} E \sin\theta \tag{13}$$

2.2.2 Frequency Response Characteristics of a Virtual Synchronous Machine (VSG)

The difference between the current control methods of different virtual synchronous machines mainly lies in the design of voltage and current rings and the control of reactive power, the common point is that the phase control is determined by the rotor motion equation in the controller, which is the core of the virtual synchronous machine. Therefore, without loss of generality, this paper assumes that the virtual synchronous machine adopts the dual-loop control structure of voltage outer ring current inner ring and reactive power-voltage sag control. Moreover, in order to better enhance the dynamic characteristics of the system, virtual impedance is added to the control of the virtual synchronous machine.

Similarly, since the frequency disturbance rejection capability of the system is investigated in this paper, the system output is chosen to be:

$$\Delta y_{VSG} = \Delta \omega_{VSG} \tag{14}$$

Perturbation input Δu is added to the phase, i.e:

$$\begin{cases} \Delta\theta = \dfrac{2\pi f_0 \Delta\omega_{VSG}}{s} + \Delta u_{VSG} \\ 2H_{VSG} s\Delta\omega_{VSG} = \Delta P_0 - \Delta P_{EVSG} - D\Delta\omega_{VSG} \end{cases} \tag{15}$$

It can be seen that Eq. (15) shows that the virtual synchronous machine has similar frequency response characteristics to the synchronous generator in terms of the open-loop characteristics of the rotor equations of motion.

2.2.3 Effect of Moment of Inertia and Damping Coefficient on the Characteristics of VSGs

The VSG controls studied in this paper are all carried out in the grid-connected state of the line, so after ignoring the inner-loop control delay, the active control loop can be simplified as shown in Fig. 3. Where K_P is the simplified synchronous power with the size of EU/Z, and Z is the sum of the virtual impedance of the VSG, the line impedance, and other fractional impedances. In this paper, K_P is assumed to be a fixed known quantity for ease of analysis.

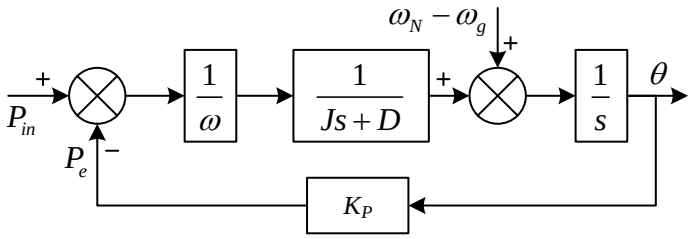

Figure 3: Structure of P control loop in grid-connected mode

(In the figure: P_m is subtracted from P_e and divided by ω, then passed through $\frac{1}{Js+D}$, added with $\omega_N - \omega_s$, and divided by s to get θ, and P_e is obtained from θ through K_P.)

The open-loop transfer function and closed-loop transfer function of the active control loop at grid-connection can be obtained from Fig:

$$G_{Po}(s) = \frac{K_P}{J\omega_N s^2 + D\omega_N s} \tag{16}$$

$$G_{Pc}(s) = \frac{P_e}{P_m} = \frac{K_P}{J\omega_N s^2 + D\omega_N s + K_P} \tag{17}$$

It can be found that the closed-loop transfer function corresponding to the active loop is a typical second-order model, then the natural oscillation angular frequency ω_n and the damping ratio ξ corresponding to the second-order model can be obtained as:

$$\begin{cases} \omega_n = \sqrt{\dfrac{K_P}{J\omega_N}} \\ \xi = \dfrac{D}{2}\sqrt{\dfrac{\omega_N}{JK_P}} \end{cases} \tag{18}$$

Assuming that $0 < \xi < 1$ and the error band is $\pm 5\%$, the maximum overshoot $\sigma\%$ and the regulation time t_s corresponding to this second-order system are:

$$\begin{cases} \sigma\% = e^{-\pi\xi/\sqrt{1-\xi^2}} \times 100\% \\ t_s \approx \dfrac{3.5}{\xi\omega_n} = \dfrac{7J}{D} \end{cases} \tag{19}$$

From Eq. (19), it can be obtained that the dynamic performance of the second-order model corresponding to the active ring is determined by the rotational inertia J and the damping coefficient D when both the active power as well as the reactive power are given. Where the inertia J mainly has a greater effect on the rate of change of frequency and the damping D has a greater effect on the amount of deviation of frequency.

2.3 Adaptive control of virtual synchronous machines for grid-connected inverters

2.3.1 VSG grid strength adaptation analysis

The adjustment of virtual damping is related to the virtual inertia and the whole step coefficient, which is proportional to the VSG machine-end voltage and inversely proportional to the total impedance of the power grid.The operating point of VSG is related to the strength of the power grid and the actual output power, and the voltage at the machine-end of the VSG is affected by the operating point, and the voltage of the power distribution network usually fluctuates within 10%, therefore, when the strength of the power grid is certain, and the actual output power of the VSG is changed, the change in the voltage at the machine-end of the VSG is not significant, and the influence on the whole step coefficient is small. Therefore, when the grid strength is certain, if the actual output power of VSG varies, the magnitude of the VSG machine-end voltage change with the operating point is not significant, and the influence on the whole-step coefficient is small, so the whole-step coefficient is mainly influenced by the total impedance of the grid. If the whole step coefficient of the VSG for parameter tuning under the set grid strength is S_{E0}, and the whole step coefficient under the actual grid-connected operation is S_{E1}, the closed-loop transfer function of the small-signal model of the VSG in the actual operation state can be expressed as:

$$G_p(s) = \frac{\Delta P_e^*}{\Delta P_M^*} = \frac{S_{E1}\omega_n}{Hs^2 + \sqrt{2HS_{E0}\omega_n}s + S_{E1}\omega_n} \tag{20}$$

The actual damping ratio of the system can be obtained as:

$$\xi' = \frac{\sqrt{2S_{E0}\omega_n / H}}{2\sqrt{S_{E1}\omega_n / H}} = \frac{1}{\sqrt{2}}\sqrt{\frac{S_{E0}}{S_{E1}}} \tag{21}$$

It can be seen that when the actual grid strength of VSG operation is smaller than the grid strength referenced by the parameter setting, i.e., $S_{E1} < S_{E0}$, then $\xi > 0.707$, the damping ratio increases, and when the difference between the grid strength is large, there is a significant overdamping, which prevents the VSG from responding to the changes in the grid more quickly; On the contrary, when the actual grid strength of VSG operation is larger than the grid strength referenced by the parameter setting, i.e., $S_{E1} > S_{E0}$, $\xi < 0.707$, the damping ratio becomes smaller, the VSG exhibits obvious under-damping characteristics, and the overshooting becomes larger, which may bring negative impacts on the grid, and thus fails to satisfy the requirement of the VSG to switch between the large power grid and the microgrid and other power grids with different strengths. The demand of the VSG is not satisfied.

2.3.2 Grid impedance detection method based on power perturbation method

Regarding the grid impedance detection methods for grid-connected inverters, they are categorized as follows: harmonic injection method, power perturbation method, LCL resonance method, recursive estimation method, and other methods. Considering that the harmonic injection method will introduce harmonic components into the grid, which will lead to the degradation of power quality, the LCL resonance method and recursive estimation method have low accuracy, and the VSGs can conveniently and actively regulate the output power, this paper adopts the power perturbation method, which detects the voltage and current responses of the common connection point PCC and the system frequency when the power perturbation occurs under the conditions of different VSG operating points, and then calculates the grid impedance.

2.3.3 Adaptive Optimization Method for VSG Parameters

According to a certain grid strength rated VSG parameters, when the actual operation of the grid strength becomes stronger, the natural frequency of the system becomes smaller and the response speed becomes faster; when the actual operation of the grid strength becomes weaker, the natural frequency of the system becomes larger and the response speed becomes slower. Therefore, the response speed of VSG is not uniform before and after the change of grid strength, and thus the inertia time constant and damping of VSG are considered to be optimized adaptively at the same time, so that the VSG has more uniform response characteristics under different grid strengths.

Taking the VSG inertia time constant $H = H_0$ at a certain grid strength S_{E0} as a benchmark, adaptive optimization of H is performed, if the grid impedance detected in the actual operating state is calculated to give the actual whole step factor of S_E and the inertia time constant of H, we have:

$$\begin{cases} \omega_{s0}^2 = S_{E0}\omega_n / H_0 \\ \omega_s^2 = S_E\omega_n / H \end{cases} \tag{22}$$

If we want to satisfy the same speed of VSG response under 2 different grid strength conditions, the natural frequency of the system corresponding to the 2 conditions is kept constant, so there is:

$$H = H_0 S_E / S_{E0} \tag{23}$$

2.4 Parameterization

2.4.1 Determination of parameters KJ and KD

The clusters of root trajectories of the active ring for different rotational inertia J and damping coefficient D can be obtained according to the active ring transfer function equation as shown in Fig. 4. From the figure, it can be seen that the root trajectory of D increases from 0 to infinity when J is 0.02, 0.06 and 0.09, respectively. S_1 and S_2 are a pair of conjugate complex roots of the system, moving in the direction shown by the arrows in the figure, and also in the direction of the slow increase of D from 0. It can be found that as D increases, S_1 and S_2 move to the left side of the complex plane at the same time, indicating that at this time the dynamics of the system is better, and the system is in an underdamped state for attenuated oscillations, with a certain degree of overshooting; however, as D continues to increase S_1 and S_2 gradually on the real axis converge, the imaginary part becomes 0, which corresponds to the critical damping state of the system; if D continues to increase, both S_1 and S_2 will move in the opposite direction on the real axis, and at this time the system is in an over-damped state, which will result in an increase in the regulation time of the system, and therefore the damping coefficient D cannot be too large. On the other hand, from the figure, it can be found that with the growth of J, the separation point of the characteristic roots S_1 and S_2 gradually tends to 0, i.e., it gradually moves to the imaginary axis, which results in the slowing down of the system's response, so the rotational inertia J cannot be too large either.

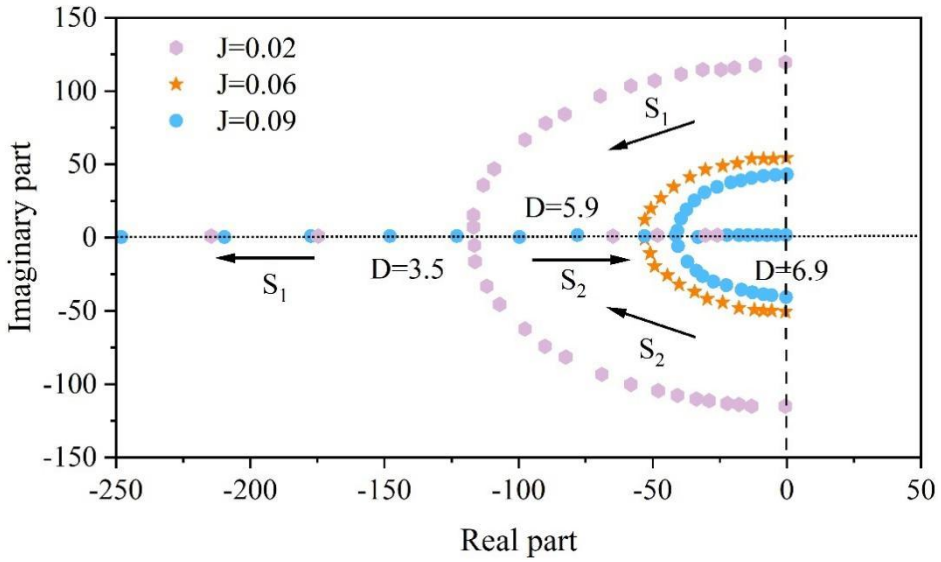

Figure 4: Root locus with different J and D

The constraint equations between inertia J and D are derived, and the selection ranges of J and D are given. Therefore, the adaptive inertia and damping of the control strategy proposed in this paper should satisfy the parameter selection range, which can be obtained as $J_{\max}$ and $D_{\max}$.

The range of inertia and damping adjustment coefficients is:

$$\begin{cases} K_J \le \dfrac{J_{\max} - J_0}{[\Delta f\,(df\ /\ dt)]_{\max}} \\ K_D \le \dfrac{D_{\max} - D_0}{[\Delta f\,(df\ /\ dt)]_{\max}} \end{cases} \tag{24}$$

Substituting the data gives $K_J \le 0.75$ and $K_D \le 3.05$.

2.4.2 Determination of parameters TJ and TD

When the VSG is in normal operation, the frequency of the system will have a small fluctuation, but the rate of change of the frequency is not negligible. T_J is used as the deviation rate threshold of frequency to judge whether to carry out the switching switch of adaptive inertia or not, in order to avoid misoperation during normal operation, T_J must be larger than the maximum value of frequency deviation rate during normal operation of VSG, and at the same time, in order to improve the accuracy of the adaptive system, T_J can not be too large, therefore only need to satisfy the avoidance of misoperation. The deviation threshold of frequency T_D can be obtained by the same reason.

3 Simulation verification

In this paper, the example is based on Matlab/Simulink simulation system to carry out model simulation analysis, and the simulation results to verify the rationality and effectiveness of the proposed adaptive control strategy, the model structure of the example system is shown in Figure 5.

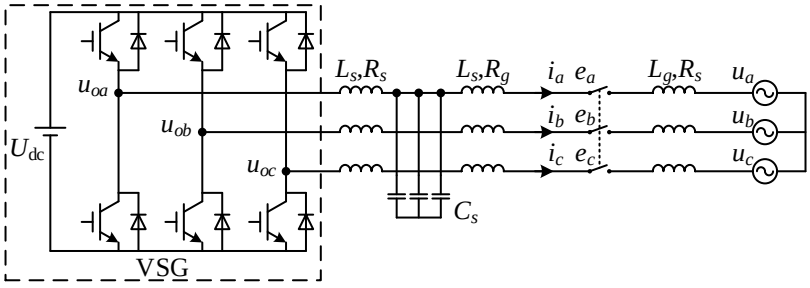

Figure 5: The topology of the calculation example VSG

The important parameters selected for the example system are as follows: the DC side of the system has a voltage of 700V and the phase voltage on the AC side of the system is 220V; Filtering parameters are set at values of $L_s = 2\,\text{mH}$, $C = 40\,\mu\text{F}$, and $R_s = 0.2\,\Omega$; Line parameters: $L_g = 2\,mH$, $R_g = 0.2\,\Omega$; Frequency difference threshold $\Delta f_{\max} = 1\,Hz$; Frequency difference rate of change threshold $k = 0.1\,Hz$; System virtual inertia $J_0 = 0.2\,kg \cdot m^2$; System damping coefficient $D_0 = 1\,N \cdot m \cdot s / rad$.

3.1 Analysis of results

3.1.1 Effect of adjustment factor on frequency fluctuation

In order to analyze the effect of different regulation coefficients on frequency stability, the virtual synchronous generator is given an active power of 5kW, K_j is taken to be K_d = 0 when it changes, and K_d is taken to be K_j=0 when it changes, and frequency fluctuations are shown in Figure 6.

From the figure, it can be seen that when the regulation coefficient K_j is 0.07, 0.1, 0.3 respectively, the time to reach the first oscillation peak is 0.09s, 0.11s, 0.13s; with the increase of K_j, the rate of change of the rotor frequency of virtual synchronous generator decreases gradually; when the regulation coefficient K_d are 6, 12 and 21, the overshoot is about 0.178Hz, 0.17Hz and 0.14Hz, respectively; as K_d increases, the overshoot of the rotor frequency gradually decreases.

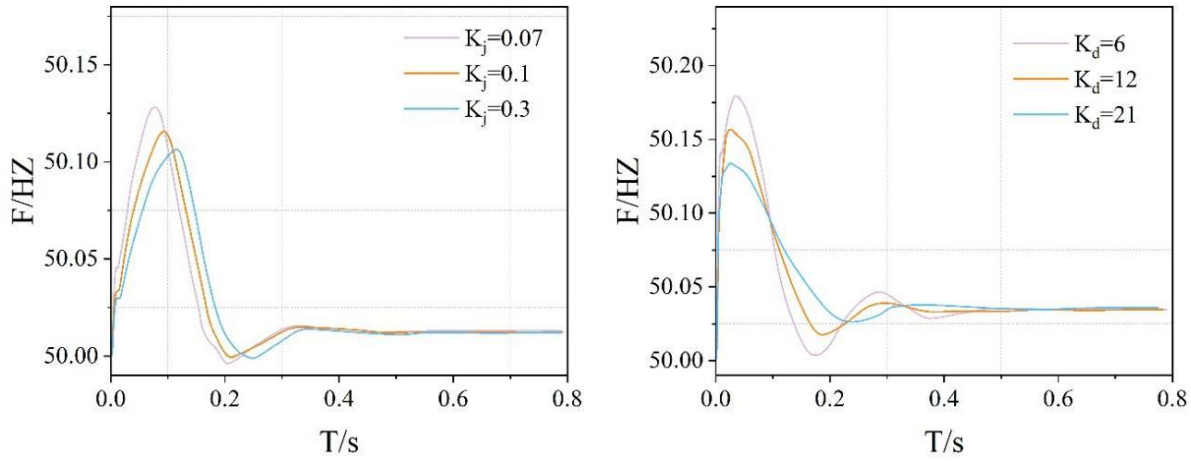

(a) K_j is different (b) K_d is different

Figure 6: Frequency fluctuation underdifferent adjustment coefficients

3.1.2 Cooperative adaptive control of moment of inertia and damping coefficients

A stand-alone virtual synchronous generator is used to connect to the grid, the simulation time is 1.6s, the active power of the load is 12kW, and the reactive power is 2kvar, the given output active power of the virtual synchronous generator is 2kW at the initial time, and the active power is suddenly increased to 12kW at 0.15s, and then suddenly decreased to 2kW at 0.9s, and the reactive power is constant at 2kvar.

Fig. 7 shows the step response curves of the virtual synchronous generator output active power under different control strategies. When the input power increases suddenly, the active overshoots with constant parameter virtual synchronous generator control (pink), rotational inertia adaptive control (yellow) and damping coefficient coordinated adaptive control (blue) are 35%, 18%, and 6%, respectively, and the regulation time is about 0.57s, 0.57s, respectively, 0.5s.

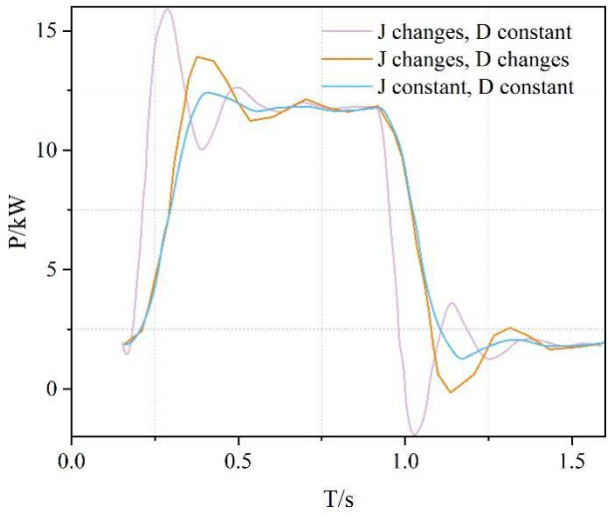

Figure 7: Comparison of active power underdifferent control strategies

Fig. 8 shows the comparison of the output frequency of the virtual synchronous generator under different control strategies. From Fig. 8(a), it can be seen that the adaptive change of rotational inertia has a significant effect on the frequency change rate. When the input power increases suddenly, the frequency deviation of the output frequency of the virtual synchronous generator under the fixed control parameter is more than 0.4 Hz, and the duration of the oscillation is about 0.27 s. When the rotational inertia adaptive control strategy is adopted, the maximum deviation of the frequency is reduced to 0.23 Hz, and the regulating time is reduced, but not obviously. Fig. 8(b) compares the output frequencies of the J adaptive virtual synchronous generator control and the J and D cooperative adaptive control, and it can be seen that the introduction of the damping coefficient adaptive control further reduces the frequency deviation, and when the frequency deviation is more than 0.1 Hz, the D adaptive increase suppresses the frequency deviation significantly.

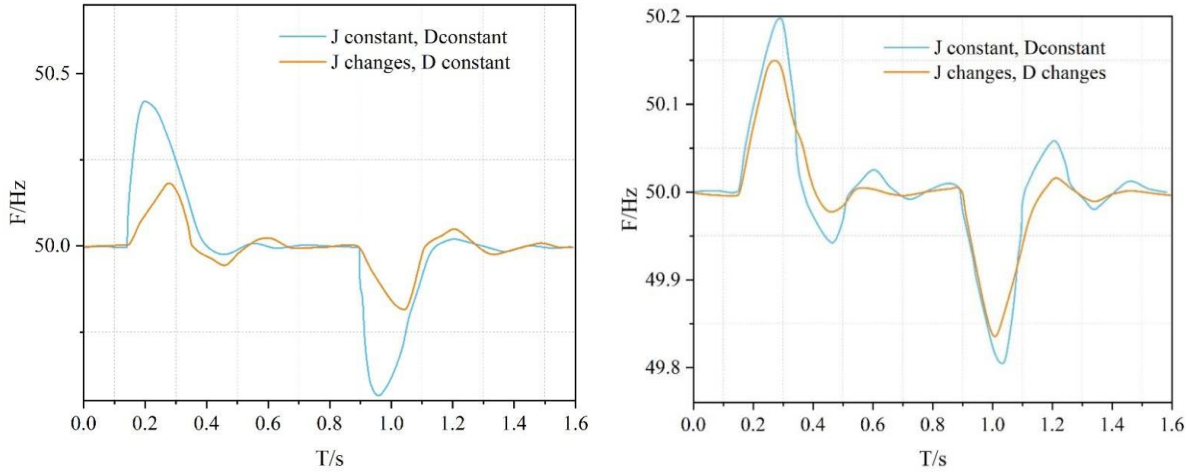

(a) Comparison between constant parameter VSG control and J adaptive VSG control

(b) Comparison between adaptive VSG control and J, D coordinated adaptive control

Figure 8: Comparison of frequency underdifferent control strategies

The variation of J and D under the cooperative adaptive control strategy of rotational inertia and damping coefficient is given in Fig. 9. The phenomenon of spikes during the change of

rotational inertia is caused by the non-smooth change of the virtual rotor frequency, which is caused by the sudden change of d_ω / d_t at the frequency inflection point.

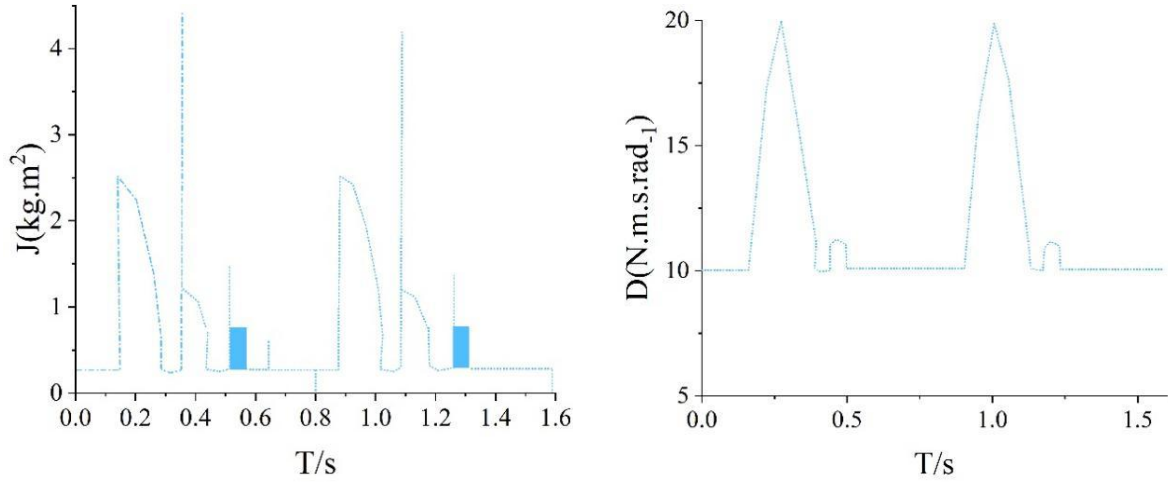

(a) Rotational inertia J (b) Damping coefficient D

Figure 9: Change of inertia and VSG

In summary, compared with the rotational inertia adaptive control, J and D cooperative adaptive virtual synchronous generator control has better frequency fluctuation suppression performance, which is able to reduce the rate of change of frequency fluctuation as well as the frequency offset, and ultimately reduce the frequency overshooting, shorten the recovery time, and improve the frequency stability performance.

3.2 Consider the operation of the system after a load disturbance

Increasing the system operation duration, when the system load changes, considering the degree of inertia of the system itself, its corresponding generation and load imbalance and other factors will lead to the frequency shift of the system. At t=2.0s, the system load decreases abruptly from 10kW to 4kW. Then the impact of the system under the three control strategies on the system is shown in Fig. 10 to Fig. 12.

From Fig. 10, it can be seen that when the load of the system fluctuates, considering the weak inertia characteristics of the system itself, the frequency stability of the VSC system can be improved by utilizing the coordinated adaptive control and strategy, and after the transient process of load fluctuation from Fig. 11, it can be seen that after the utilization of the coordinated adaptive control strategy, the active output of the system can be smoothly transitioned to the new steady state; from Fig. 12, it can be seen that under the coordinated adaptive control strategy proposed in this paper, the system corresponds to the new steady state; from Fig. 12, it can be seen that the system corresponds to the new steady state. Adaptive control strategy, the system corresponds to the DC side voltage drops to 0.99 (the youngest value) after the start of the recovery, while the constant inertia + constant damping control strategy corresponds to the DC side voltage drops to 0.96 (the youngest value) before the start of the recovery, the use of the virtual inertia adaptive strategy corresponds to the DC side voltage to drop to 0.98 (the youngest value) before the recovery. It can be summarized that after the system load fluctuation, the coordinated adaptive control strategy can make the system quickly return to a stable state, thus verifying the transient performance of the system under load disturbance.

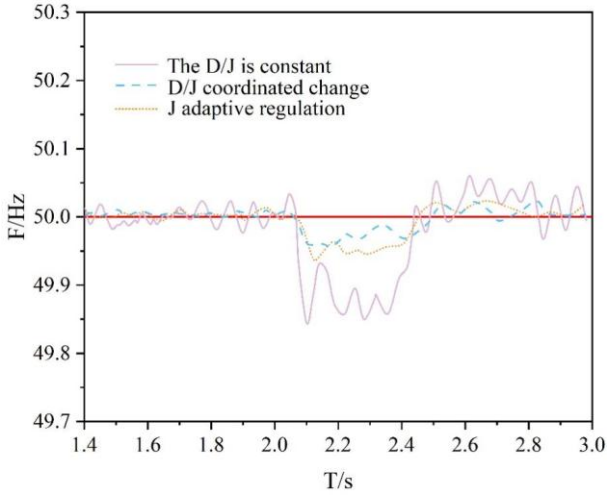

Figure 10: Effect of load change on system frequency

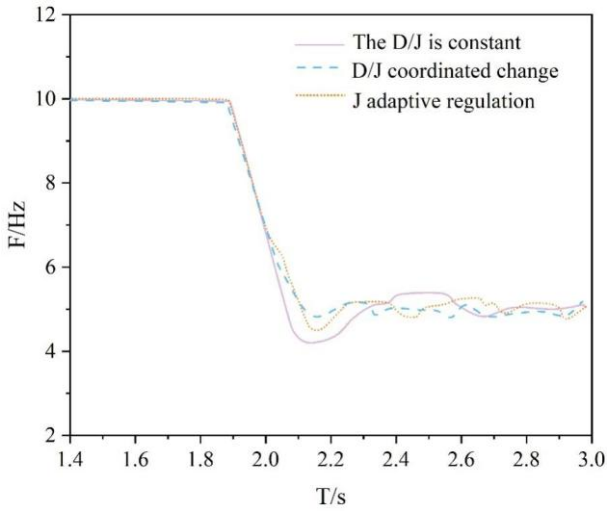

Figure 11: Effect of load changes on system active power

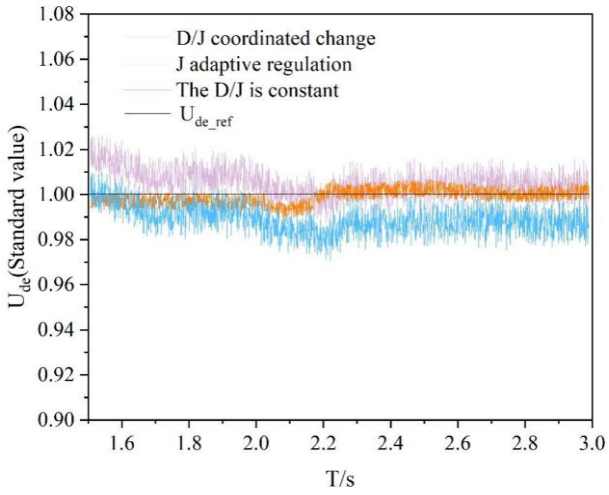

Figure 12: Effect of load change on system DC voltage

4 Conclusion

Aiming at the stability problem due to power perturbation when a large number of power sources of photovoltaic power plants are connected to the grid, this paper proposes the adaptive virtual inertia and damping control strategy method, models and analyzes the conventional VSG, analyzes the principle and feasibility of this control strategy that can improve the adaptability of the VSG power grid, and obtains the following conclusions:

(1) The adaptive virtual inertia and damping control strategy not only takes into account the change of rotational inertia, but also the change of damping coefficient, which suppresses the rate of change of frequency as well as the amount of frequency deviation, and at the same time, compared with the conventional virtual synchronous generator control and the adaptive control strategy of rotational inertia, the control strategy proposed in this paper is able to further improve the frequency response characteristics of the power supply and the output active response characteristics.

(2) The control strategy set up in this paper can effectively suppress the transient response time of the system, and compared with other control strategies, the adaptive virtual inertia and damping control strategy method can make the system corresponding to the DC side voltage drop to 0.99, which improves the stability and reliability of the system.

About the Author

Lihui Tian is a College of Electrical Engineering, Shanghai University of Electric Power. Her research focuses on the Low-frequency wind power grid connection.

References

[1] Triguero-Ruiz, F., Avila-Cano, A., & Aranda, F. T. (2023). Measuring the diversification of energy sources: The energy mix. Renewable Energy, 216, 119096.

[2] Maradin, D. (2021). Advantages and disadvantages of renewable energy sources utilization. International Journal of Energy Economics and Policy, 11(3), 176-183.

[3] Мельник, Л., Дериколенко, О., Мазін, Ю., Маценко, О., & Півень, В. (2020). Modern Trends in the Development of Renewable Energy: the Experience of the EU and Leading Countries of the World. Mechanism of an economic regulation, (3 (89)), 117-133.

[4] Hayat, M. B., Ali, D., Monyake, K. C., Alagha, L., & Ahmed, N. (2019). Solar energy—A look into power generation, challenges, and a solar-powered future. International journal of energy research, 43(3), 1049-1067.

[5] Jiang, S., Wan, C., Chen, C., Cao, E., & Song, Y. (2018). Distributed photovoltaic generation in the electricity market: status, mode and strategy. CSEE Journal of Power and Energy Systems, 4(3), 263-272.

[6] El-houari, H., Allouhi, A., Rehman, S., Buker, M. S., Kousksou, T., Jamil, A., & El Amrani, B. (2019). Design, simulation, and economic optimization of an off-grid photovoltaic system for rural electrification. Energies, 12(24), 4735.

[7] de Faria Jr, H., Trigoso, F. B., & Cavalcanti, J. A. (2017). Review of distributed generation

with photovoltaic grid connected systems in Brazil: Challenges and prospects. Renewable and Sustainable Energy Reviews, 75, 469-475.

[8] Wu, X., Yang, C., Han, W., & Pan, Z. (2022). Integrated design of solar photovoltaic power generation technology and building construction based on the Internet of Things. Alexandria Engineering Journal, 61(4), 2775-2786.

[9] Narkwatchara, P., Ratanatamskul, C., & Chandrachai, A. (2021). Performance analysis of electricity generation from grid-connected photovoltaic system using All-Sky Index for Smart City projects in Thailand. Renewable Energy, 171, 315-327.

[10] Yang, Y., Ma, C., Lian, C., Zhang, Y., & Pang, X. (2021). Optimal power reallocation of large-scale grid-connected photovoltaic power station integrated with hydrogen production. Journal of cleaner production, 298, 126830.

[11] Numbi, B. P., & Malinga, S. J. (2017). Optimal energy cost and economic analysis of a residential grid-interactive solar PV system-case of eThekwini municipality in South Africa. Applied Energy, 186, 28-45.

[12] Tan, C., Teng, X., Ding, Q., Xiao, X., Lan, Q., Cao, R., & Chang, L. (2022). Synergistic balancing control for low-inertia power systems with high PV penetration: Tibet as a case study. Energy Reports, 8, 2924-2935.

[13] Wamukoya, B. K., Kaberere, K. K., & Muriithi, C. M. (2025). Optimal deployment of solar PV power plants as fast frequency response source for a frequency secure low inertia power grid. Bulletin of Electrical Engineering and Informatics, 14(1), 83-95.

[14] Huang, X., Wang, K., Li, G., & Zhang, H. (2018). Virtual inertia-based control strategy of two-stage photovoltaic inverters for frequency support in islanded micro-grid. Electronics, 7(11), 340.

[15] Zhang, Y., Liu, X., Wu, Y., Wang, S. E., Wang, Y., Tang, Z., ... & Hao, J. (2019, November). Analysis of inertia mechanism of grid-tied photovoltaic power generation system with virtual inertia control. In 2019 4th IEEE Workshop on the Electronic Grid (eGRID) (pp. 1-6). IEEE.

[16] Yue, M., & Wang, X. (2014). Grid inertial response-based probabilistic determination of energy storage system capacity under high solar penetration. IEEE transactions on sustainable energy, 6(3), 1039-1049.

[17] Saadatmand, M., Gharehpetian, G. B., Moghassemi, A., Guerrero, J. M., Siano, P., & Alhelou, H. H. (2021). Damping of low-frequency oscillations in power systems by large-scale PV farms: A comprehensive review of control methods. IEEE Access, 9, 72183-72206.

[18] Hosseinipour, A., & Hojabri, H. (2018). Virtual inertia control of PV systems for dynamic performance and damping enhancement of DC microgrids with constant power loads. IET Renewable Power Generation, 12(4), 430-438.

[19] Wu, F., Yang, B., Hu, A., Zhang, Y., Ge, W., Ni, L., ... & Zha, Y. (2021). Inertia and damping analysis of grid-tied photovoltaic power generation system with DC voltage

droop control. IEEE Access, 9, 38411-38418.

[20] Duc Tuan Do & Honnyong Cha. (2025). High-reliability single-phase current source inverter with switching-cell structure for grid-connected photovoltaic systems. Journal of Power Electronics,25(3),1-12.